

Supporting Information

Highly Stable Lanthanide Cluster-based Luminescent Materials Constructed from β -diketone to 1,10-phenanthroline Exhibiting Ultrahigh Photoluminescence and Efficient Pesticide Detection

Mei-Xin Hong,^{a†} Cheng Chen,^{a†} Lingyun Cao,^{b*} Jun Zheng,^a and Xiu-Ying Zheng^{a*}

^a Institutes of Physical Science and Information Technology, Key Laboratory of Structure and Functional Regulation of Hybrid Materials of Ministry of Education, Anhui University, Hefei, 230601, P. R. China.

^b Innovation Laboratory for Sciences and Technologies of Energy Materials of Fujian Province (IKKEM), Xiamen, 361005, P. R. China.

E-mail: caoly@xmu.edu.cn, xyzheng@ahu.edu.cn

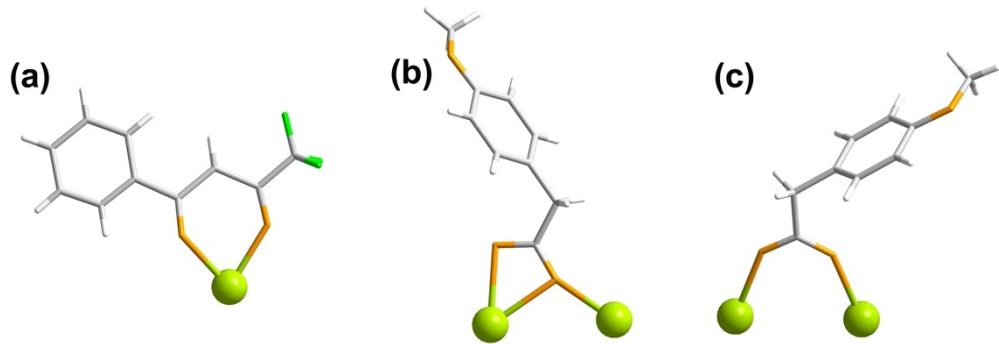


Fig. S1 The coordination modes of (a) bfta^- and (b) mpa^- lignads in compounds **Eu_{2b}** and **Eu_{2p}**. Green Ln; yellow O, grey C, white, H.

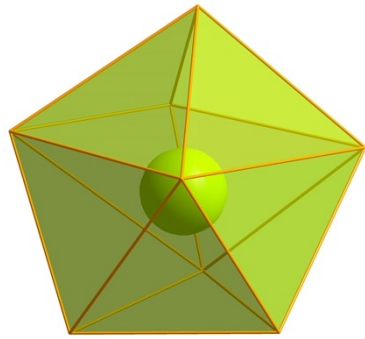


Fig. S2 The snub diphenoid geometry of the octa-coordinated Eu^{3+} in **Eu_{2b}**.

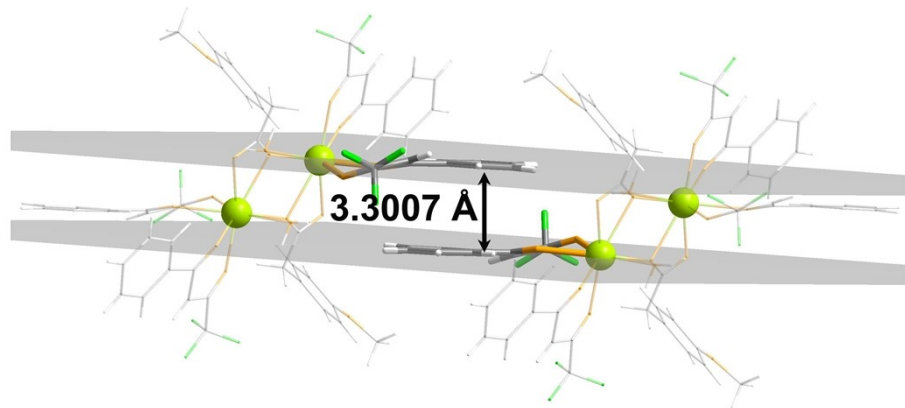


Fig. S3 The vertical distance between the two planes formed by the benzene rings on the two adjacent bfta^- ligands in **Eu_{2b}**.

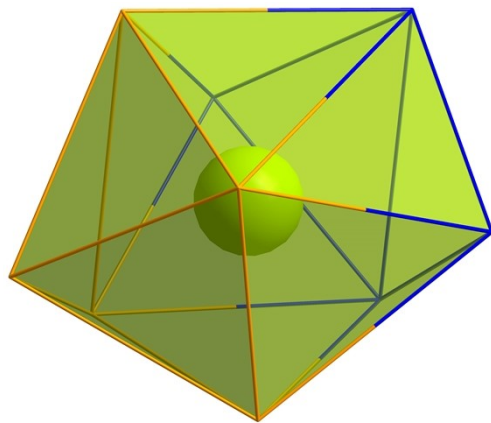


Fig. S4 The tricapped trigonal prism geometry of nona-coordinated Eu³⁺ in Eu_{2p}.

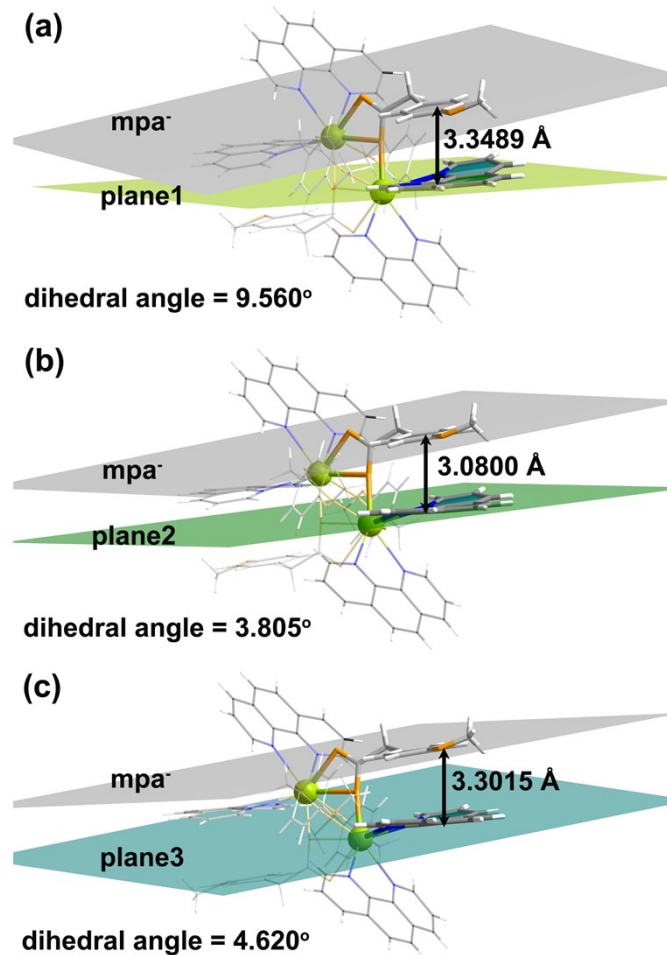


Fig. S5 (a, b, c) In compound Eu_{2p}, the dihedral angles between the three planes (plane1, plane2, plane3) in phen1 and the plane of the benzene ring in mpa⁻, and the vertical distances from the centers of the plane1, plane2 and plane3 in phen1 to the plane of the benzene ring in mpa⁻.

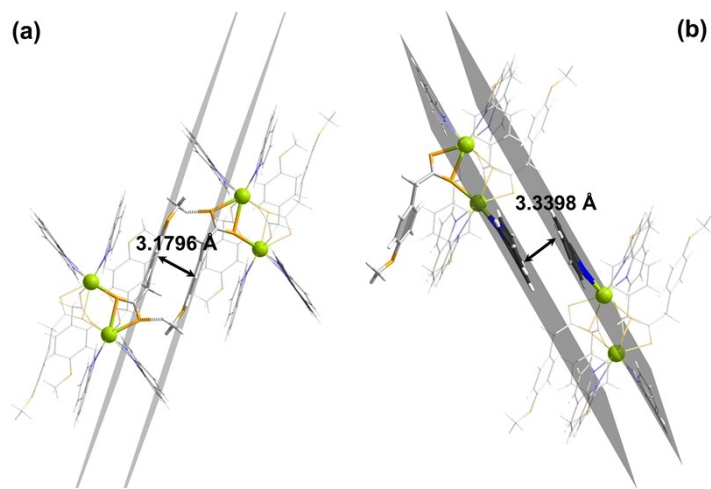


Fig. S6 The vertical distance between the adjacent planes of two mpap^- ligands (a), and that of two phen_2 ligands (b).

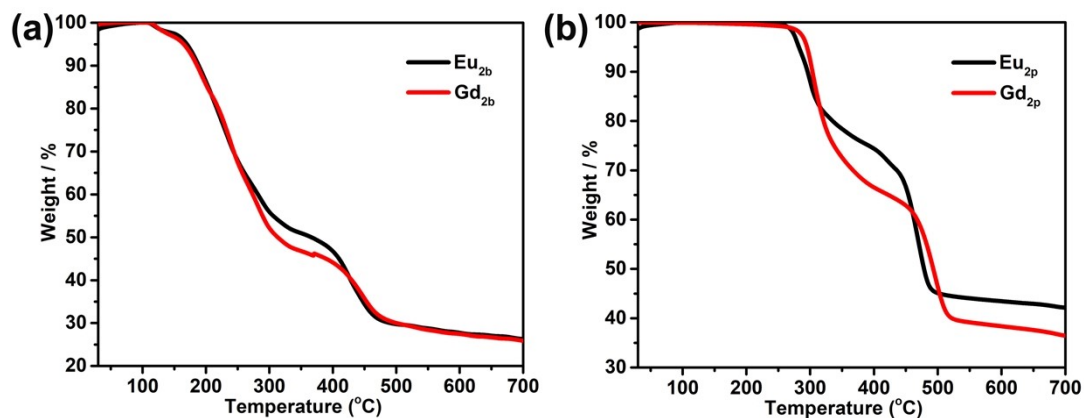


Fig. S7 The TGA of (a) compounds Eu_{2b} , Gd_{2b} and (b) compounds Eu_{2p} , Gd_{2p} under nitrogen atmosphere.

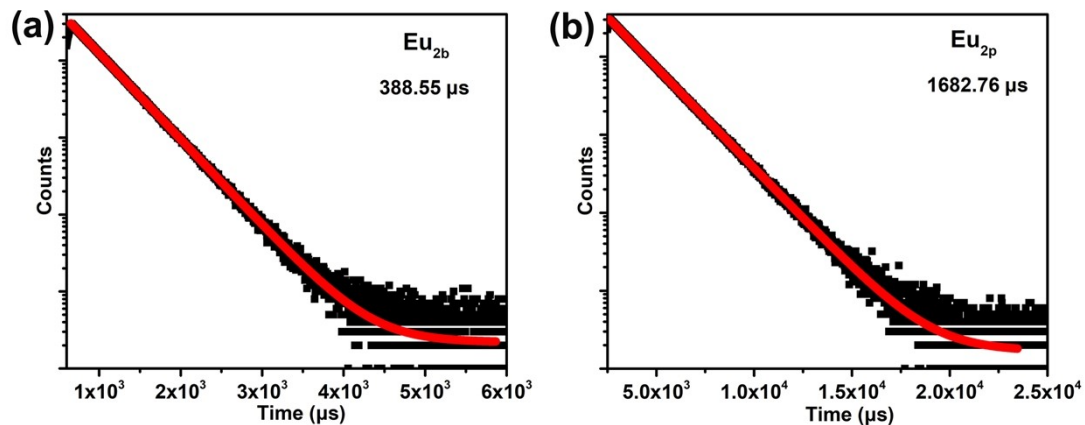


Fig. S8 The decay curves of (a) compounds Eu_{2b} and (b) Eu_{2p} .

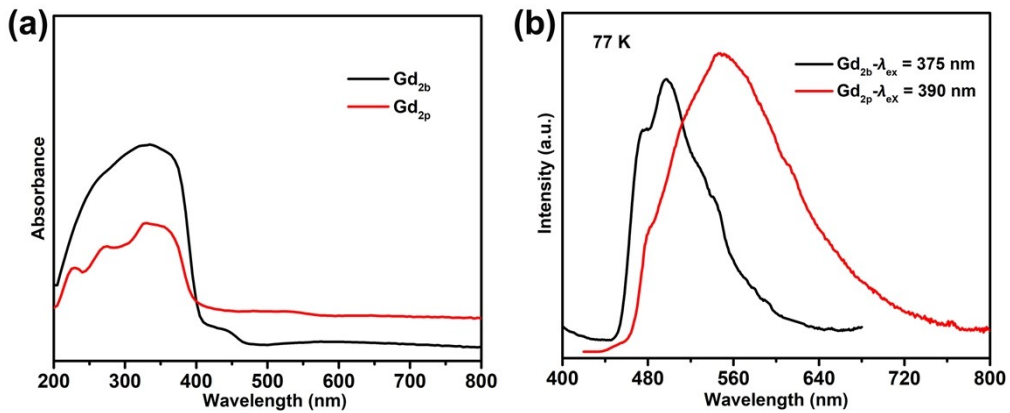


Fig. S9 (a) The solid-state UV-vis spectra of Gd_{2b} and Gd_{2p} at room temperature; (b) the solid-state phosphorescence emission spectra of Gd_{2b} and Gd_{2p} at 77 K.

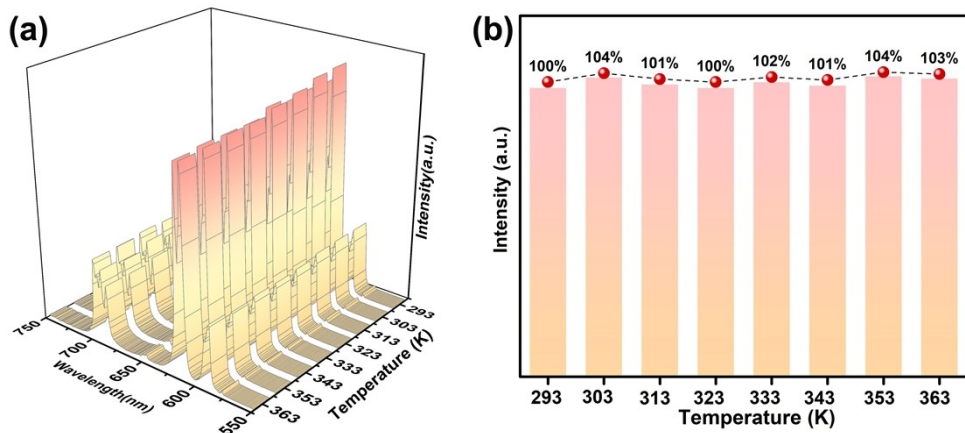


Fig. S10 (a) The temperature-dependent emission spectra of $\text{Eu}_{2p}@\text{PMMA}$; (b) the emission intensity (anchored at 614 nm) of $\text{Eu}_{2p}@\text{PMMA}$ from 293 to 363 K.

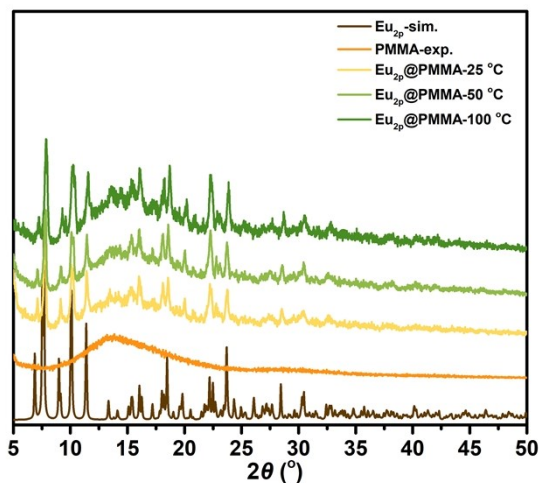


Fig. S11 Time-dependent PXRD patterns of $\text{Eu}_{2p}@\text{PMMA}$ from 25 to 100 $^\circ\text{C}$.

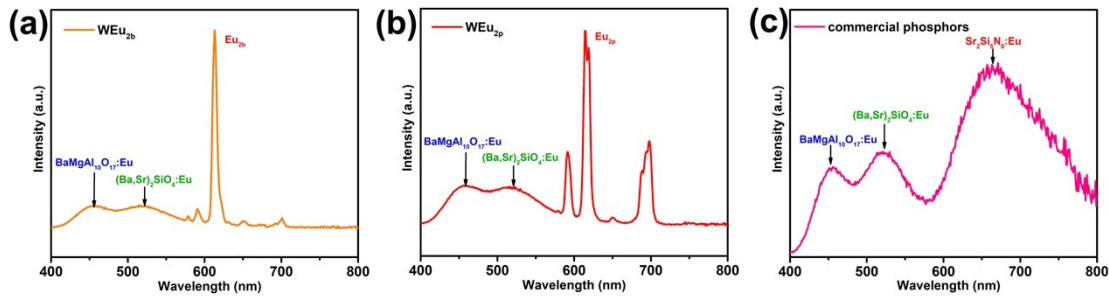


Fig. S12 The emission spectra of $\text{WEu}_{2\text{b}}$, $\text{WEu}_{2\text{p}}$ and the mixed commercial phosphors.

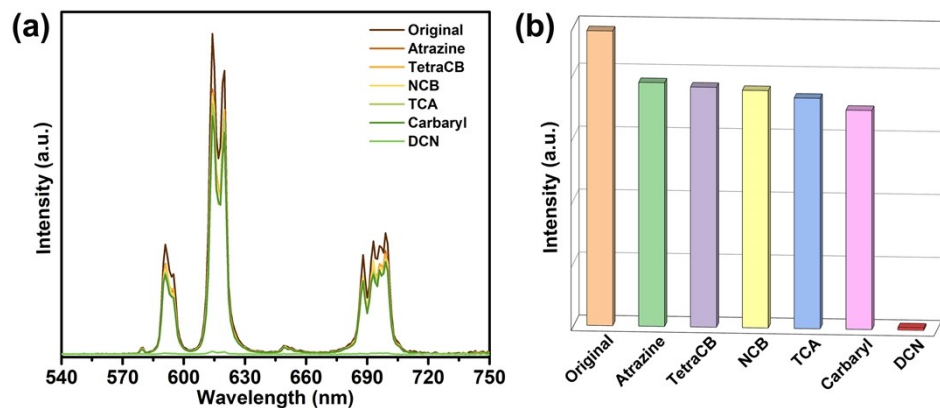


Fig. S13 The emission spectra (a) and the emission intensity (b, anchored at 614 nm) of $\text{Eu}_{2\text{p}}$ toward different pesticides in EtOH solution.

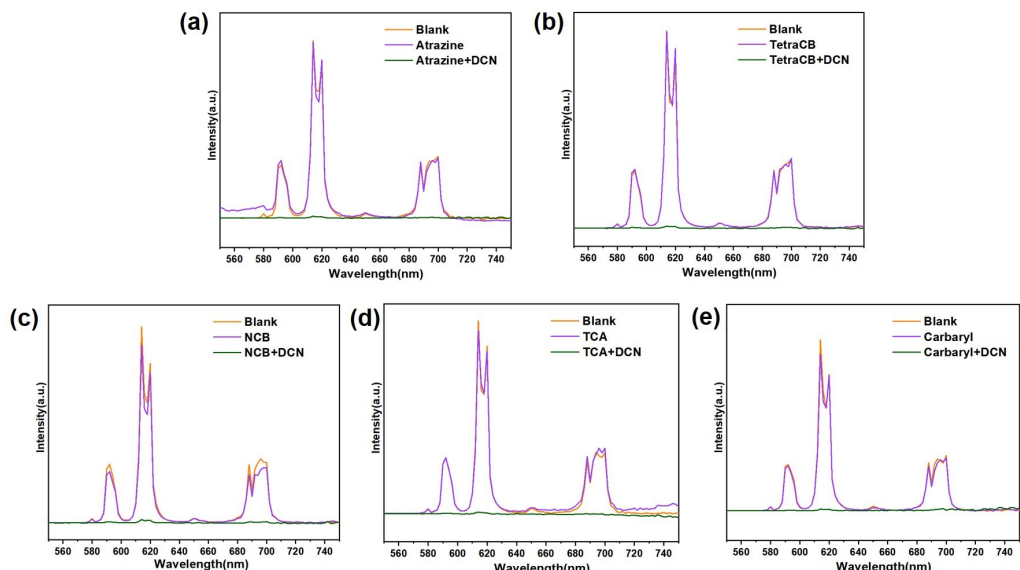


Fig. S14 The emission spectra of the selectivity experiment of $\text{Eu}_{2\text{p}}$ toward DCN in the presence of other different pesticides.

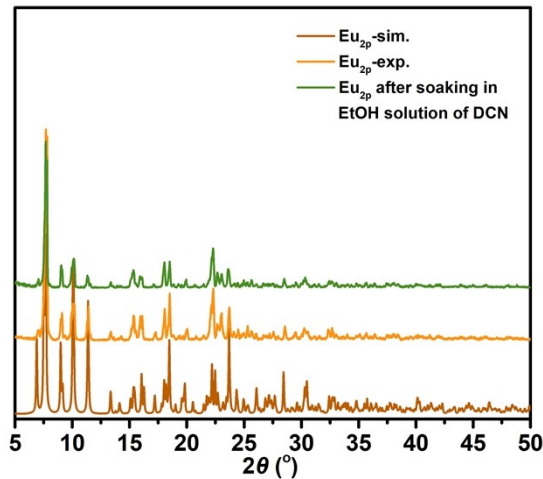


Fig. S15 The PXRD patterns of Eu_{2p} before and after soaking in EtOH solution of DCN.

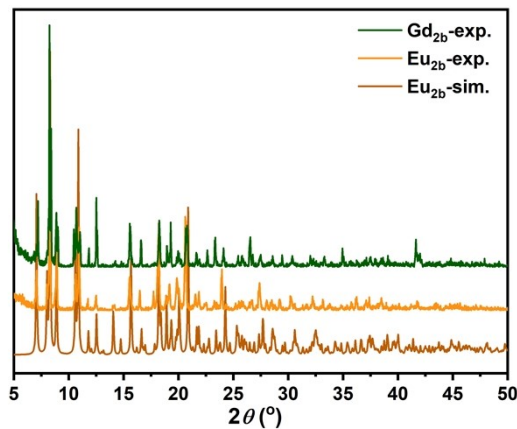


Fig. S16 The PXRD patterns of Eu_{2b} and Gd_{2b} .

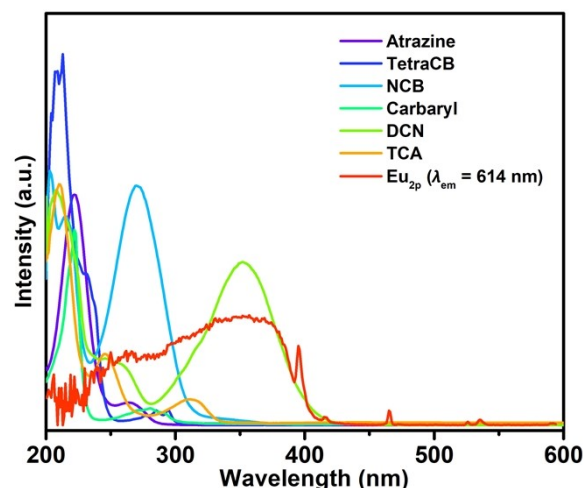


Fig. S17 The absorption spectra of different pesticides in EtOH solution and the

excitation spectrum of **Eu_{2p}** at $\lambda_{\text{em}} = 614$ nm.

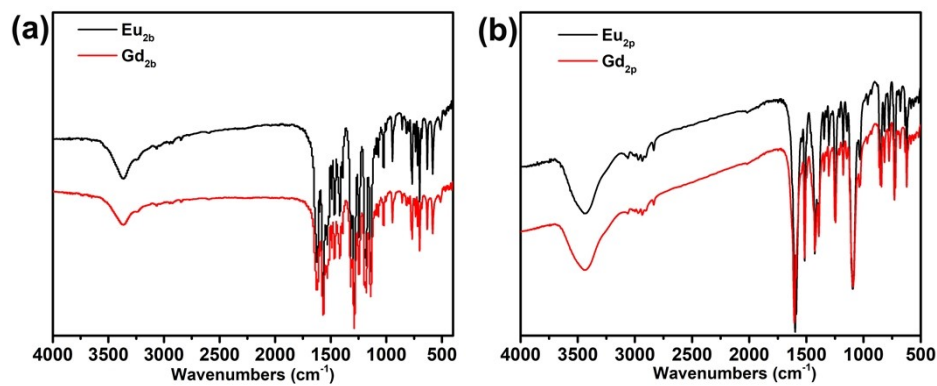


Fig. S18 IR spectra in 500 – 4000 cm⁻¹ for (a) **Eu_{2b}**, **Gd_{2b}** and (b) **Eu_{2p}**, **Gd_{2p}**.

Table S1. Crystallographic Data for Compounds **Eu₂b**, **Gd₂b**.

compound	Eu₂b	Gd₂b
Formula	C ₅₈ H ₄₆ Eu ₂ F ₁₂ O ₁₆	C ₅₈ H ₄₆ Gd ₂ F ₁₂ O ₁₆
FW	1530.87	1541.45
T/K	120	120
Cry. System	triclinic	triclinic
Space group	<i>P</i> -1	<i>P</i> -1
<i>a</i> /Å	10.1101(15)	10.1164(17)
<i>b</i> /Å	12.1486(17)	12.138(2)
<i>c</i> /Å	13.7123(18)	13.680(2)
α / °	112.931(10)	112.871(11)
β / °	93.700(11)	93.806(13)
γ / °	97.746(12)	97.821(14)
<i>V</i> /Å ³	1524.3(4)	1520.2(4)
Z	1	1
Dc /g cm ⁻³	1.668	1.684
μ / mm ⁻¹	15.489	14.872
Data/parameters	5434/399	5415/399
2θ / °	7.058 - 139.04	8.03 - 139.19
Obs. reflections	13374	20545
F (000)	756.0	758.0
GOOF	1.101	1.011
R ₁ [I > 2σ(I)] ^a	0.0971	0.0409
wR ₂ (All data) ^b	0.1198	0.0501

^aR₁= $\sum||FO| - |F_C||/\sum|F_O|$; ^bwR₂= $\{\sum[w(F_O^2 - F_C^2)^2]/\sum[w(F_O^2)^2]\}^{1/2}$

Table S2. Crystallographic Data for Compounds **Eu_{2p}**, **Gd_{2p}**.

compound	Eu_{2p}	Gd_{2p}
Formula	C ₈₄ H ₇₂ Cl ₂ Eu ₂ N ₈ O ₂₂	C ₈₄ H ₇₂ Cl ₂ Gd ₂ N ₈ O ₂₂
FW	1920.31	1930.89
T / K	120	150
Cry. System	triclinic	triclinic
Space group	<i>P</i> -1	<i>P</i> -1
<i>a</i> / Å	11.970	11.9791(14)
<i>b</i> / Å	12.237	12.2597(14)
<i>c</i> / Å	13.604	13.6056(18)
α / °	75.15	74.888(10)
β / °	75.36	75.411(10)
γ / °	79.39	79.339(9)
<i>V</i> / Å ³	1848.3	1851.5(4)
Z	1	1
D _c / g cm ⁻³	1.725	1.732
μ / mm ⁻¹	13.426	12.862
Data/parameters	6209/525	6723/525
2θ / °	6.886 - 129.998	6.89 - 139.376
Obs. reflections	18605	27933
F (000)	988.0	1000.0
GOOF	1.027	1.010
R ₁ [I > 2σ(I)] ^a	0.0374	0.0328
wR ₂ (All data) ^b	0.0917	0.0745

^aR₁= $\sum||FO| - |F_C||/\sum|F_O|$; ^bwR₂= $\{\sum[w(F_O^2 - F_C^2)^2]/\sum[w(F_O^2)^2]\}^{1/2}$

Table S3. Selected bond distances (\AA) and band angles ($^\circ$) of **Eu_{2b}**.

Eu1-Eu1 ¹	4.0620(15)	O2-C12	1.188(11)
Eu1-O2	2.354(8)	O4-C4	1.275(12)
Eu1-O3	2.458(8)	O5-C15	1.231(11)
Eu1-O4 ¹	2.472(9)	F2-C25	1.319(16)
Eu1-O5	2.311(9)	F3-C28	1.331(14)
Eu1-O6	2.378(9)	O6-C9	1.238(11)
Eu1-O7	2.360(9)	O7-C10	1.200(11)
Eu1-O8 ¹	2.489(8)	O8-C4	1.276(12)
Eu1-O8	2.409(8)	F4-C25	1.320(12)
Eu1-C4 ¹	2.875(6)	F5-C28	1.356(19)
O1-C1	1.350(16)	F6-C25	1.341(17)
O1-C26	1.419(17)	C1-C8	1.39(2)
F1-C28	1.322(13)	C1-C21	1.396(18)
<hr/>			
O2-Eu1-Eu1 ¹	147.8(2)	O3-Eu1-O8 ¹	78.2(3)
O2-Eu1-O3	75.3(3)	O3-Eu1-C4 ¹	76.4(3)
O2-Eu1-O4 ¹	87.2(3)	O4 ¹ -Eu1-Eu1 ¹	84.7(2)
O2-Eu1-O6	136.0(3)	O4 ¹ -Eu1-O8 ¹	52.4(3)
O2-Eu1-O7	71.9(3)	O4 ¹ -Eu1-C4 ¹	26.2(3)
O2-Eu1-O8	134.4(3)	O5-Eu1-Eu1 ¹	115.9(2)
O2-Eu1-O8 ¹	134.8(3)	O5-Eu1-O2	72.6(3)
O2-Eu1-C4 ¹	110.7(3)	O5-Eu1-O3	100.2(3)
O3-Eu1-Eu1 ¹	72.6(2)	O5-Eu1-O4 ¹	158.8(3)
O3-Eu1-O4 ¹	80.4(3)	O5-Eu1-O6	83.9(3)

Symmetry code: ¹-X,1-Y,-Z

Table S4. Selected bond distances (\AA) and band angles ($^\circ$) of **Gd_{2b}**.

Gd1-Gd1 ¹	4.0474(10)	O4-C13	1.275(7)
Gd1-O1 ¹	2.446(4)	O5-C2	1.377(6)
Gd1-O2	2.342(3)	O5-C27	1.431(6)
Gd1-O3	2.370(3)	F1-C20	1.328(7)
Gd1-O4	2.303(4)	O6-C12	1.246(6)
Gd1-O6	2.346(3)	F2-C20	1.330(7)
Gd1-O7	2.395(3)	F3-C29	1.321(8)
Gd1-O8 ¹	2.487(3)	F4-C20	1.323(7)
Gd1-O8	2.392(3)	F5-C29	1.327(7)
Gd1-C1 ¹	2.840(5)	O8-C1	1.283(6)
O1-C1	1.250(6)	F6-C29	1.346(8)
O2-C28	1.255(6)	C1-C8	1.509(7)
O3-C26	1.288(6)	C2-C7	1.393(7)
<hr/>			
O1 ¹ -Gd1-Gd1 ¹	84.88(8)	O2-Gd1-C1 ¹	110.12(13)
O1 ¹ -Gd1-O8 ¹	52.75(11)	O3-Gd1-Gd1 ¹	75.73(8)
O1 ¹ -Gd1-C1 ¹	26.02(13)	O3-Gd1-O1 ¹	107.54(13)
O2-Gd1-Gd1 ¹	147.82(8)	O3-Gd1-O7	146.61(12)
O2-Gd1-O1 ¹	86.85(12)	O3-Gd1-O8	74.82(11)
O2-Gd1-O3	136.26(12)	O3-Gd1-O8 ¹	81.42(11)
O2-Gd1-O6	71.68(12)	O3-Gd1-C11	96.65(14)
O2-Gd1-O7	75.49(12)	O4-Gd1-Gd1 ¹	115.76(9)
O2-Gd1-O8 ¹	134.75(11)	O4-Gd1-O1 ¹	158.75(12)
O2-Gd1-O8	134.44(11)	O4-Gd1-O2	72.97(12)

Symmetry code: ¹-X,1-Y,-Z

Table S5. Selected bond distances (\AA) and band angles ($^\circ$) of Eu_{2p} .

Eu1-Eu1 ¹	3.9414(5)	O1-C1	1.269(5)
Eu1-O1 ¹	2.380(3)	O2-C2	1.281(5)
Eu1-O2	2.344(3)	O3-C1	1.249(5)
Eu1-O2 ¹	2.641(3)	O4-C2	1.254(5)
Eu1-O3	2.383(3)	O5-C9	1.424(6)
Eu1-O4 ¹	2.430(3)	O5-C13	1.375(5)
Eu1-N1	2.579(3)	N1-C8	1.363(5)
Eu1-N2	2.635(3)	N1-C34	1.336(5)
Eu1-N3	2.634(4)	N2-C3	1.360(5)
Eu1-N4	2.636(4)	N2-C33	1.320(5)
Eu1-C2 ¹	2.912(4)	N3-C23	1.361(6)
Cl1-O7	1.419(4)	N3-C26	1.332(6)
Cl1-O8	1.411(4)	O6-C30	1.371(6)
O1 ¹ -Eu1-Eu1 ¹	68.56(7)	O2 ¹ -Eu1-Eu1 ¹	35.19(6)
O1 ¹ -Eu1-O2 ¹	71.67(9)	O2-Eu1-O1 ¹	74.90(10)
O1 ¹ -Eu1-O3	137.88(9)	O2-Eu1-O2 ¹	75.67(10)
O1 ¹ -Eu1-O4 ¹	75.83(10)	O2-Eu1-O3	75.62(10)
O1 ¹ -Eu1-N1	81.16(10)	O2-Eu1-O4 ¹	124.88(10)
O1 ¹ -Eu1-N2	132.55(10)	O2-Eu1-N1	142.97(10)
O1 ¹ -Eu1-N3	137.70(10)	O2-Eu1-N2	150.75(10)
O1 ¹ -Eu1-N4	75.80(10)	O2-Eu1-N3	99.64(10)
O1 ¹ -Eu1-C2 ¹	74.05(10)	O2-Eu1-N4	76.11(10)
O2-Eu1-Eu1	40.48(7)	O2 ¹ -Eu1-C2 ¹	26.08(10)

Symmetry code:¹1-X,-Y,1-Z

Gd1-Gd1 ¹	3.9340(7)	C11-O9	1.411(4)
Gd1-O1	2.366(2)	C11-O10	1.417(5)
Gd1-O2 ¹	2.422(3)	O1-C8	1.255(4)
Gd1-O3 ¹	2.368(2)	O2-C2	1.239(4)
Gd1-O5 ¹	2.639(2)	O3-C8	1.261(4)
Gd1-O5	2.338(2)	O4-C3	1.375(5)
Gd1-N1	2.621(3)	O4-C26	1.430(5)
Gd1-N2	2.623(3)	O5-C2	1.282(4)
Gd1-N3	2.565(3)	N1-C4	1.367(5)
Gd1-C2 ¹	2.903(4)	N1-C25	1.331(5)
Gd1-N4	2.614(3)	N2-C7	1.327(5)
C11 -O7	1.429(3)	N2-C15	1.372(5)
C11-O8	1.410(4)	N3-C1	1.371(5)

O1-Gd1-Gd1 ¹	69.21(6)	O2 ¹ -Gd1-N1	65.48(9)
O1-Gd1-O2 ¹	97.46(9)	O2 ¹ -Gd1-N2	137.70(9)
O1-Gd1-O3 ¹	137.86(8)	O2 ¹ -Gd1-N3	74.22(9)
O1-Gd1-O5 ¹	72.14(8)	O2 ¹ -Gd1-C2 ¹	24.88(9)
O1-Gd1-N1	75.87(9)	O2 ¹ -Gd1-N4	132.95(9)
O1-Gd1-N2	124.57(9)	O3 ¹ -Gd1-Gd1 ¹	68.80(6)
O1-Gd1-N3	138.35(9)	O3 ¹ -Gd1-O2 ¹	75.71(9)
O1-Gd1-C21	82.88(9)	O3 ¹ -Gd1-O5 ¹	71.76(8)
O1-Gd1-N4	76.90(9)	O3 ¹ -Gd1-N1	132.36(9)
O2 ¹ -Gd1-Gd1 ¹	85.19(6)	O3 ¹ -Gd1-N2	75.58(9)
O2 ¹ -Gd1-O5 ¹	50.90(8)	O3 ¹ -Gd1-N3	80.67(9)

Table S6. Selected bond distances (Å) and band angles (°) of **Gd₂p**.

Symmetry code: $^{11}-X,-Y,1-Z$

Table S7. The CShM (Continuous Shape Measurements) values of Ln^{3+} ions with octa-coordinate mode in compounds **Eu_{2b}**, **Gd_{2b}**.

Refcode ^a	Com. ^b	Eu_{2b}	Gd_{2b}
		Eu1	Gd1
OP-8		24.391	24.579
HPY-8		16.733	16.875
HBPY-8		13.713	13.703
CU-8		13.432	13.431
SAPR-8		7.619	7.572
TDD-8		6.271	6.356
JGBF-8		11.602	11.527
JETBPY-8		20.865	20.846
JBTPR-8		5.395	5.375
BTPR-8		6.432	6.44
JSD-8		4.332	4.326
TT-8		14.056	14.064
ETBPY-8		21.262	21.396

^aOP-8, Octagon; HPY-8, Heptagonal pyramid; HBPY-8, Heptagonal bipyramid; CU-8, Cube; SAPR-8, Square antiprism; TDD-8, Triangular dodecahedron; JGBF-8, Johnson gyrobifastigium; JETBPY-8, Johnson elongated triangular bipyramid; JBTPR-8, Biaugmented trigonal prism; BTPR-8, Biaugmented trigonal prism; JSD-8, Snub diphenoïd; TT-8, Triakis tetrahedron; ETBPY-8, Elongated trigonal bipyramid.

^bLanthanide ions in each asymmetric unit of compounds **Eu_{2b}**, **Gd_{2b}**.

Table S8. The CShM (Continuous Shape Measurements) values of Ln^{3+} ions with nona-coordinate mode in compounds $\text{Eu}_{2\text{p}}$, $\text{Gd}_{2\text{p}}$.

Refcode ^a	Com. ^b	$\text{Eu}_{2\text{p}}$	$\text{Gd}_{2\text{p}}$
		Eu1	Gd1
EP-9		25.227	25.192
OPY-9		20.08	20.055
HBPY-9		16.932	16.953
JTC-9		14.295	14.233
JCCU-9		12.166	12.144
CCU-9		12.202	12.188
JCSAPR-9		4.596	4.603
CSAPR-9		4.511	4.525
JTCTPR-9		4.259	4.213
TCTPR-9		5.092	5.137
JTDIC-9		14.36	14.425
HH-9		10.87	10.876
MFF-9		4.394	4.416

^aEP-9, Enneagon; OPY-9, Octagonal pyramid; HBPY-9, Heptagonal bipyramid; JTC-9, Johnson triangular cupola; JCCU-9, Capped cube; CCU-9, Spherical-relaxed capped cube; JCSAPR-9, Capped square antiprism; CSAPR-9, Spherical capped square antiprism; JTCTPR-9, Tricapped trigonal prism; TCTPR-9, Spherical tricapped trigonal prism; JTDIC-9, Tridiminished icosahedron; HH-9, Hula-hoop; MFF-9, Muffin. ^bLanthanide ions in each asymmetric unit of compounds $\text{Eu}_{2\text{p}}$, $\text{Gd}_{2\text{p}}$.

Table S9. Some lanthanide compounds with high quantum yields.

Lanthanide compounds	QY	Ref.
Eu(hfa) ₃ (TPPO) ₂	65%	1
[Eu(tftpa) _{1.5} (bpy)(H ₂ O)] _n	74.50%	2
[Eu ₂ (m-BDC) ₃ (Phen) ₂] DMF	75%	3
[Eu ₂ (2,3'-oba) ₃ (phen) ₂] _n	75.57%	4
[Eu(hfac) ₃ (DPEPO)]	80%	5
{[Eu(H ₂ O)(TPA)(ox)]·0.5H ₂ O}	89%	6
n		
[Eu(phen) ₂ (NO ₃) ₃]	90%	7
{[EuKL ₄ (H ₂ O) ₂]·H ₂ O} _n	92%	8
[Eu(pfbz) ₂ (phen)Cl]	97.70%	9
Eu₂p	96.79%	This work

Table S10. Some metal compounds for DCN detection.

Metal compounds	K_{sv} (M^{-1})	LOD	Ref.
Eu ₂ (dtztp)-MOF	6.25×10^4	5.28 ppm	10
Tb ₃ (HDDB)(DDB)(H ₂ O) ₆	6.42×10^4	$1.4 \times 10^{-7} M$	11
[Cd ₁₈ Sm ₆ L ₉ (OAc) ₃₆]	2.45×10^4	$6.7 \times 10^{-7} M$	12
[Ag(CIP ⁻)]	5.2×10^4	$1.7 \times 10^{-7} M$	13
[Ag(3-dpyb)(H ₃ odpa)]·H ₂ O	2.028×10^5	$1.154 \times 10^{-6} M$	14
[Cd(tptc) _{0.5} (bpz)-CP]	4.71×10^4	112 ppb	15
[Cd ₃ (CBCD) ₂ (DMA) ₄ (H ₂ O) ₂]·10DMA	4.47×10^4	145 ppb	16
[Mg ₂ (APDA) ₂ (H ₂ O) ₃]·5DMA·5H ₂ O	7.5×10^4	150 ppb	17
Eu_{2p}	3.21×10^4	$1.21 \times 10^{-7} M$	This work

References:

- (1) K. Miyata, Y. Hasegawa, Y. Kuramochi, T. Nakagawa, T. Yokoo, T. Kawai, Characteristic Structures and Photophysical Properties of Nine-Coordinate Europium (III) Complexes with Tandem-Connected Tridentate Phosphane Oxide Ligands, *Eur. J. Inorg. Chem.* 2009, **2009**, 4777-4785.
- (2) Y. Xiao-Bo, C. Zhao, M. Yuan-Jie, L. Ling, W.-T. CHANG, L. Bo, Z. Cheng-Hui, Synthesis of highly luminescent LnMOFs through structural regulation, *Chinese J. Struct. Chem.* 2022, **41**, 2203270-2203276.
- (3) S. Zou, Q. Li, S. Du, Efficient and tunable multi-color and white light Ln-MOFs with high luminescence quantum yields, *RSC Adv.* 2015, **5**, 34936-34941.
- (4) J.-M. Li, R. Li, X. Li, Construction of metal–organic frameworks (MOFs) and highly luminescent Eu(III)-MOF for the detection of inorganic ions and antibiotics in aqueous medium, *CrystEngComm* 2018, **20**, 4962-4972.
- (5) M. Congiu, M. Alamiry, O. Moudam, S. Ciorba, P. R. Richardson, L. Maron, A. C. Jones, B. S. Richards, N. Robertson, Preparation and photophysical studies of [Ln(hfac)₃DPEPO], Ln= Eu, Tb, Yb, Nd, Gd; interpretation of total photoluminescence quantum yields., *Dalton Trans.* 2013, **42**, 13537-13545.
- (6) H.-W. Yang, P. Xu, B. Ding, X.-G. Wang, Z.-Y. Liu, H.-K. Zhao, X.-J. Zhao, E.-C. Yang, Design, Isostructural lanthanide coordination polymers with high photoluminescent quantum yields by effective ligand combination: crystal structures, photophysical characterizations, biologically relevant molecular sensing, and anti-counterfeiting ink application, *Cryst. Growth Des.* 2020, **20**, 7615-7625.

- (7) M. Liu, Z. Li, J. Xiong, Y. Jiang, T. Tang, J. Qiu, J. Yao, S. W. Ng, C. Zeng, Structure regulation for ultra-high luminescence quantum yield lanthanide complex and simultaneous detection of cancer marker and ferrous ion, *J. Rare Earths* 2021, **39**, 1194-1203.
- (8) K. Zheng, Z. Liu, Y. Jiang, P. Guo, H. Li, C. Zeng, S. W. Ng, S. Zhong, Ultrahigh luminescence quantum yield lanthanide coordination polymer as a multifunctional sensor, *Dalton Trans.* 2018, **47**, 17432-17440.
- (9) M.-Y. Ye, M.-X. Zhang, Q.-F. Xu, H. Xu, L.-S. Long, L.-S. Zheng, Highly stable Eu-coordination polymer exhibiting the highest quantum yield, *Sci. China Chem.* 2023, **66**, 1400-1405.
- (10) G.-D. Wang, Y.-Z. Li, W.-J. Shi, B. Zhang, L. Hou, Y.-Y. Wang, A robust cluster-based Eu-MOF as multi-functional fluorescence sensor for detection of antibiotics and pesticides in water, *Sensors Actuators B: Chemical* 2021, **331**, 129377.
- (11) X.-Q. Wang, X. Ma, D. Feng, J. Tang, D. Wu, J. Yang, J. Jiao, Four novel lanthanide (III) metal-organic frameworks: Tunable light emission and multiresponsive luminescence sensors for vitamin B6 and pesticides, *Cryst. Growth Des.* 2021, **21**, 2889-2897.
- (12) Y. Cheng, Y. Ma, X. Yang, H. Li, Z. Zhang, D. Schipper, A 24-metal Cd (II)-Sm (III) nanocage with a rapid triple-emissive response for 2, 6-dichloro-4-nitroaniline, *Inorg. Chem. Front.* 2023, **10**, 417-423.
- (13) D.-D. Feng, Y.-D. Zhao, X.-Q. Wang, D.-D. Fang, J. Tang, L.-M. Fan, J. Yang, Two novel metal-organic frameworks based on pyridyl-imidazole-carboxyl

multifunctional ligand: selective CO₂ capture and multiresponsive luminescence sensor, *Dalton Trans.* 2019, **48**, 10892-10900.

(14) J. Ma, Y. Wang, G. Liu, N. Xu, X. Wang, A pH-stable Ag (I) multifunctional luminescent sensor for the efficient detection of organic solvents, organochlorine pesticides and heavy metal ions, *RSC Adv.* 2020, **10**, 44712-44718.

(15) L. Fan, F. Wang, D. Zhao, X. Sun, H. Chen, H. Wang, X. Zhang, Two cadmium (II) coordination polymers as multi-functional luminescent sensors for the detection of Cr (VI) anions, dichloronitroaniline pesticide, and nitrofuran antibiotic in aqueous media, *Spectrochimica Acta Part A: Molecular Biomolecular Spectroscopy* 2020, **239**, 118467.

(16) N. Xu, Q. Zhang, G. Zhang, A carbazole-functionalized metal-organic framework for efficient detection of antibiotics, pesticides and nitroaromatic compounds, *Dalton Trans.* 2019, **48**, 2683-2691.

(17) N. Xu, Q. Zhang, B. Hou, Q. Cheng, G. Zhang, A novel magnesium metal-organic framework as a multiresponsive luminescent sensor for Fe(III) ions, pesticides, and antibiotics with high selectivity and sensitivity, *Inorg. Chem.* 2018, **57**, 13330-13340.